An Impactor Origin for Lunar Magnetic Anomalies

Mark A. Wieczorek, *et al.*

Science **335**, 1212 (2012);
DOI: 10.1126/science.1214773

Science (print ISSN 0036-8075; online ISSN 1095-9203) is published weekly, except the last week in December, by the American Association for the Advancement of Science, 1200 New York Avenue NW, Washington, DC 20005.

more inert host and hence a loss in activity. However, there are now many experimental and theoretical examples of metal alloys under realistic conditions in which the more active element is stabilized at the surface by adsorbates (*21*, *30*–*32*). This adsorbate-induced reverse segregation effect is understood in terms of the adsorbate binding more strongly to the element, which would normally segregate to the bulk and result in a reversal of the surface segregation behavior (*21*). In the case of the Cu/Pd system, the stabilization resulting from segregation of Cu to the surface is small (0.02 eV) (*31*) compared with the ~0.4-eV increase in binding of H to Pd versus Cu (*6*, *20*). The fact that Pd segregation to the Cu surface has been observed experimentally in Pd/Cu catalysts under realistic hydrogenation operating conditions bodes well for the utility of this atomic geometry in real catalysts (*32*).

References and Notes

1. S. Abbet *et al.*, *J. Am. Chem. Soc.* **122**, 3453 (2000).
2. J. C. Fierro-Gonzalez, V. A. Bhirud, B. C. Gates, *Chem. Commun.* **42**, 5275 (2005).
3. Y. Zhai *et al.*, *Science* **329**, 1633 (2010).
4. J. M. Thomas, Z. Saghi, P. L. Gai, *Top. Catal.* **54**, 588 (2011).
5. F. Besenbacher *et al.*, *Science* **279**, 1913 (1998).
6. H. L. Tierney, A. E. Baber, J. R. Kitchin, E. C. H. Sykes, *Phys. Rev. Lett.* **103**, 246102 (2009).
7. D. O. Bellisario *et al.*, *J. Phys. Chem. C* **113**, 12863 (2009).
8. H. L. Tierney, A. E. Baber, E. C. H. Sykes, *J. Phys. Chem. C* **113**, 7246 (2009).
9. Methods and additional data are available as supporting material on *Science* Online.
10. A. Bach Aaen, E. Lægsgaard, A. V. Ruban, I. Stensgaard, *Surf. Sci.* **408**, 43 (1998).
11. T. Kammler, J. Küppers, *J. Chem. Phys.* **111**, 8115 (1999).
12. I. S. Chopra, S. Chaudhuri, J. F. Veyan, Y. J. Chabal, *Nat. Mater.* **10**, 884 (2011).
13. A. Wittstock, V. Zielasek, J. Biener, C. M. Friend, M. Bäumer, *Science* **327**, 319 (2010).
14. L. J. Lauhon, W. Ho, *Phys. Rev. Lett.* **85**, 4566 (2000).
15. T. Mitsui, M. K. Rose, E. Fomin, D. F. Ogletree, M. Salmeron, *Nature* **422**, 705 (2003).
16. G. Anger, A. Winkler, K. D. Rendulic, *Surf. Sci.* **220**, 1 (1989).
17. G. E. Gdowski, T. E. Felter, R. H. Stulen, *Surf. Sci.* **181**, L147 (1987).
18. C. Sousa, V. Bertin, F. Illas, *J. Phys. Chem. B* **105**, 1817 (2001).
19. A. Roudgar, A. Groß, *Surf. Sci.* **597**, 42 (2005).
20. J. Greeley, M. Mavrikakis, *J. Phys. Chem. B* **109**, 3460 (2005).
21. J. Greeley, M. Mavrikakis, *Nat. Mater.* **3**, 810 (2004).
22. J. Knudsen *et al.*, *J. Am. Chem. Soc.* **129**, 6485 (2007).
23. O. Skoplyak, M. A. Barteau, J. G. Chen, *J. Phys. Chem. B* **110**, 1686 (2006).
24. S. Alayoglu, A. U. Nilekar, M. Mavrikakis, B. Eichhorn, *Nat. Mater.* **7**, 333 (2008).
25. J. T. Roberts, R. J. Madix, *J. Am. Chem. Soc.* **110**, 8540 (1988).
26. W. T. Tysoe, G. L. Nyberg, R. M. Lambert, *Chem. Commun.* **11**, 623 (1983).
27. G. Kyriakou, J. Kim, M. S. Tikhov, N. Macleod, R. M. Lambert, *J. Phys. Chem. B* **109**, 10952 (2005).
28. B. Brandt *et al.*, *J. Phys. Chem. C* **112**, 11408 (2008).
29. H.-L. Jiang, Q. Xu, *J. Mater. Chem.* **21**, 13705 (2011).
30. F. Tao *et al.*, *Science* **322**, 932 (2008).
31. D. Priyadarshini *et al.*, *J. Phys. Chem. C* **115**, 10155 (2011).
32. J. A. Anderson, M. Fernández-García, G. L. Haller, *J. Catal.* **164**, 477 (1996).

Acknowledgments: We thank the U.S. Department of Energy (FG02-10ER16170) for financial support, NSF (CBET 0828666) for partial support (M.B.B.) and for a Graduate Research Fellowship (A.D.J.), the Department of Education for a Graduate Assistance in Areas of National Need fellowship (E.A.L.), and Tufts University for a Tufts Collaborates Seed Grant (E.C.H.S., M.F.-S., and G.K.).

Supporting Online Material

www.sciencemag.org/cgi/content/full/335/6073/1209/DC1
Materials and Methods
SOM Text
Figs. S1 to S4
References (*33*–*37*)

27 October 2011; accepted 30 January 2012
10.1126/science.1215864

An Impactor Origin for Lunar Magnetic Anomalies

Mark A. Wieczorek,[1]* Benjamin P. Weiss,[2] Sarah T. Stewart[3]

The Moon possesses strong magnetic anomalies that are enigmatic given the weak magnetism of lunar rocks. We show that the most prominent grouping of anomalies can be explained by highly magnetic extralunar materials from the projectile that formed the largest and oldest impact crater on the Moon: the South Pole–Aitken basin. The distribution of projectile materials from a model oblique impact coincides with the distribution of magnetic anomalies surrounding this basin, and the magnetic properties of these materials can account for the intensity of the observed anomalies if they were magnetized in a core dynamo field. Distal ejecta from this event can explain the origin of isolated magnetic anomalies far from this basin.

Beginning with the Apollo era, spacecraft observations have shown that portions of the lunar crust are strongly magnetized (*1*–*4*), yet their origin has remained unresolved. The lithologies of the source rocks for these anomalies are unknown, their time of magnetization acquisition is poorly constrained, and it is unclear whether the magnetization process was thermoremanent or shock-related (*5*, *6*). As a result, the origin of the magnetizing fields is a matter of debate, with possibilities including a core dynamo, transient fields generated during impacts, and the amplification of ambient fields by impact-generated plasmas (*7*–*13*).

A key difficulty is that most lunar magnetic anomalies have not been recognized to correlate with known geologic structures. A few impact basins possess central magnetic anomalies (*12*, *14*, *15*), but these anomalies are typically weak and are not representative of the most intense anomalies, most of which are located on the far side of the Moon (Fig. 1). Impact basin ejecta deposits are statistically somewhat more magnetic than other geologic units, but the magnetic signatures of the ejecta from any given basin are quite variable (*16*). A few prominent anomalies on the far side of the Moon are located near the antipodes of four young impact basins (*2*, *3*), suggestive of an exotic impact origin (*17*), but many strong anomalies are not associated with basin antipodes, and most basins do not possess antipodal anomalies.

It is also difficult to reconcile the strengths of these anomalies with the magnetic properties of known endogenous lunar materials. This is because lunar materials are very weakly magnetic relative to terrestrial materials: The saturation remanent magnetizations of mare basalts and pristine highlands rocks are weaker than those of mid-ocean ridge basalt by two to four or more orders of magnitude (*18*, *19*). To demonstrate this, we calculated the thickness of magnetized materials required to generate a representative 10-nT anomaly at an altitude of 30 km as a function of the magnetizing field strength and rock thermoremanence susceptibility (ratio of thermoremanence to the magnetizing field) (Fig. 2). The thermoremanence susceptibility correlates with both the abundance of magnetic carriers in the rock and the rock's saturation remanent magnetization (supporting online material), and lunar paleomagnetic studies imply ancient field strengths between ~1 and 120 μT (*5*, *20*, *21*). We find that even the highest postulated paleofield strengths would require extremely thick deposits of unidirectionally magnetized materials to account for the lunar magnetic anomalies. For example, more than 100 km of pristine feldspathic highland rocks would be required, but these thicknesses are greater than the thickness of the entire lunar crust. More than 10 km of mare basalts would be required, but this far exceeds the thickness of most maria (*11*). Even the relatively highly magnetic mafic impact melts, most of which are thought to be derived from the Imbrium impact event (*22*), would require thicknesses of at least several kilometers, but none of the magnetic anomalies show the topographic expressions that might be expected for such locally thick ejecta deposits.

However, there is a major geologic structure that correlates with some of the largest lunar magnetic anomalies and that has received little consideration previously. The far-side hemisphere of the Moon hosts the largest known unequivocal

[1]Institut de Physique du Globe de Paris, Université Paris Diderot, 94100 Saint-Maur des Fossés, France. [2]Department of Earth, Atmospheric, and Planetary Sciences, Massachusetts Institute of Technology, Cambridge, MA 02139, USA. [3]Department of Earth and Planetary Sciences, Harvard University, Cambridge, MA 02138, USA.

*To whom correspondence should be addressed. E-mail: wieczor@ipgp.fr

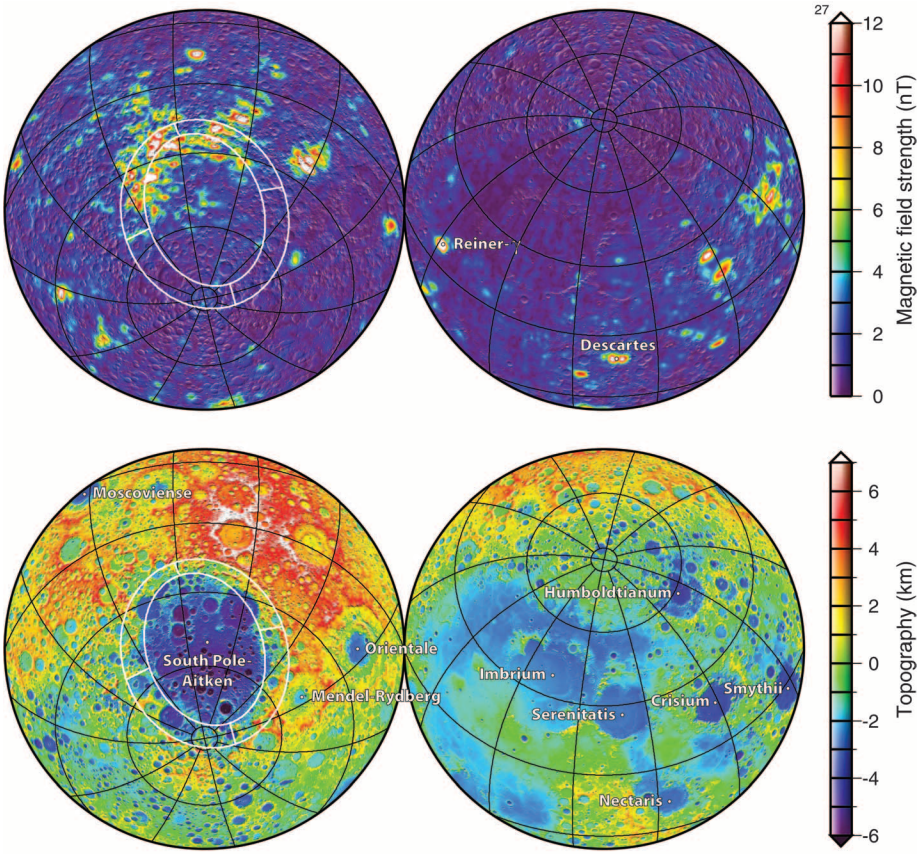

Fig. 1. Magnetic field strength and topography centered over the South Pole–Aitken basin (left) and opposite hemisphere of the Moon (right). Upper panel: Total magnetic field strength from the sequential Lunar Prospector model of (*4*) evaluated 30 km above the surface. Lower panel: Topography from Lunar Reconnaissance Orbiter laser altimeter data (*34*). Ellipses elongated in the north-south direction denote the inner basin floor and outer structural rim of the South Pole–Aitken basin (*23*), and the connecting lines join the respective semiminor and semimajor axes. All images show half of the lunar surface and are displayed in a Lambert azimuthal equal-area projection overlain by a shaded relief map derived from the surface topography.

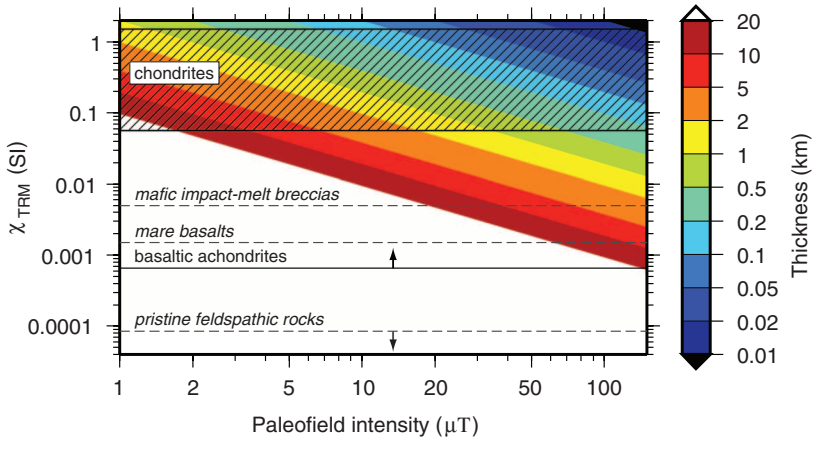

Fig. 2. Thickness of magnetic materials required to generate a 10-nT anomaly 30 km above the lunar surface. Thermoremanent magnetizations acquired in a dipolar field were determined for each thermoremanence susceptibility, χ_{TRM} (in SI units), and surface paleofield intensity within a representative disk 60 km in diameter at 30° latitude. The maximum magnetic field strength scales linearly with disk thickness, and the disk thicknesses would differ by a factor of ~2 for anomalies located at the poles and equator, or for disk diameters of 35 and 200 km. Representative thermoremanence susceptibilities of lunar (dashed) and meteoritic (solid) materials are denoted by horizontal lines (data from tables S2 and S3).

impact structure in the solar system: the South Pole–Aitken basin (Fig. 1). With a mean diameter of ~2200 km, this basin is elongated in the north-south direction and was likely formed by an oblique impact, with the projectile coming from either the north or south (*23*). The most prominent grouping of lunar magnetic anomalies coincides with the northern rim of this basin, precisely where one would expect projectile materials to have been deposited if the impact direction was from the south.

We propose that materials from the South Pole–Aitken impactor are the source materials for many of the largest lunar magnetic anomalies. With high concentrations of metallic iron and other magnetic minerals, typical projectile materials are on average about two orders of magnitude more magnetic than endogenous lunar crustal materials (Fig. 2). If the projectile was similar to a chondritic meteorite, and if these materials were magnetized by cooling in a steady core dynamo field, integrated thicknesses of only a few hundred meters would be required to account for the strength of the lunar anomalies. If the projectile was instead differentiated, the projectile core materials would have been even more magnetic than undifferentiated chondritic meteorites.

Projectile materials should be incorporated into impact deposits in abundances sufficient to substantially change the magnetic properties of these rocks. Terrestrial impact melts are known to contain materials from the impactor ranging from less than 1 weight percent (wt%) up to several wt% (*24*, *25*). The mafic impact melts sampled during the Apollo missions are thought to have formed during one or more basin-forming impact events (primarily Imbrium) and contain ~1 to 2 wt% macroscopic metallic iron that was derived from the core of a differentiated planetesimal (*22*, *26*). Given the enormous size of the South Pole–Aitken basin, the projectile that formed this basin would have been ~10 times as massive as that which formed the next largest lunar basin, and comparable in mass to all other basin-forming projectiles combined. Numerical simulations show that most of the projectile would accrete to the Moon in a molten or partially molten state for an average impact angle and velocity (*27*).

We assessed the hypothesis that projectile materials from the South Pole–Aitken impact event are responsible for the majority of lunar magnetic anomalies by tracking the fate of projectile materials in a suite of impact simulations. Our simulations used a three-dimensional Eulerian shock physics code with self-gravity and multiphase equations of state for crustal, mantle, and core materials (supporting online material). The rheologies of the target and projectile materials were dependent on pressure, temperature, and strain rate (*28*). The model Moon possessed a silicate crust 50 km thick, with a forsterite mantle and a small iron core, whereas the projectile was treated as being either homogeneous in composition or differentiated with a silicate mantle and iron core. Simulations were run for more than 1 hour after the impact, which allowed most of the ejecta to re-impact the Moon.

As a representative case, a 45° oblique impact at 15 km s^{-1} of a differentiated projectile 200 km in diameter completely excavated the crust of the Moon over an area ~1200 km in diameter and formed a thick impact melt pool in the basin interior (Fig. 3). The resulting ring of crustal thickening is similar in size to the topographic rim of the South Pole–Aitken basin, although it is not elliptical. Differences in crater shape and crustal structure between the model and observations may result from gravitational and viscous modification processes that are not accounted for in the simulations, or from the relatively low spatial resolution used to model the lunar crust. In the simulation, most of the projectile silicate mantle was vaporized and lost to space, and only ~1% of these materials were retained in the proximal ejecta. The retained projectile mantle materials were deposited downrange and exterior to the basin's excavation cavity, and possessed integrated thicknesses close to 100 m extending about one crater diameter from the basin rim. Only a negligible fraction of the projectile core was vaporized, and almost 80% of these materials were retained on the surface of the Moon. The retained projectile core materials were deposited primarily near the downrange basin rim with thicknesses up to a few kilometers.

We calculated the magnetic signature of the projectile deposits by assuming that they acquired a thermoremanence by cooling in the presence of a global dipolar field (supporting online material), although transient fields and shock remanence acquisition are also possible (*8*). The projectile mantle was modeled using the magnetic properties of basaltic achondrites, which have thermoremanence susceptibilities less than those of chondritic materials by about three orders of magnitude (Fig. 1). The magnetic properties of projectile core materials are not well known (*29*) and will depend primarily on how the projectile metal is mixed with silicate materials in the impact process (which will determine the grain sizes, shapes, and magnetostatic interactions between the metal particles). As a very conservative estimate, we used a thermoremanent susceptibility of 0.5 SI units for the core materials, which is representative of the ordinary and enstatite chondrites. Given that these chondritic materials contain only a few tens of wt% metallic iron, the true thermoremanent susceptibility of projectile core materials is probably several times our chosen value.

If the dipole field strength on the surface of the Moon was just 5 μT when this basin formed [at the low end of most paleofield estimates (*5*)], the projectile core materials would give rise to several magnetic anomalies with intensities of more than 10 nT at 30 km altitude (Fig. 3). Both the intensities and the spatial distribution of these magnetic anomalies are similar to those observed adjacent to the South Pole–Aitken basin. Although most of the strong anomalies are located near the downrange rim of the impact basin, a few strong anomalies are found exterior to the basin rim as well.

We have investigated the sensitivity of these results by testing impact angles of 30°, 45°, and 60° from vertical; impact velocities of 10, 15, and 30 km s^{-1}; and impactor diameters of 150, 200,

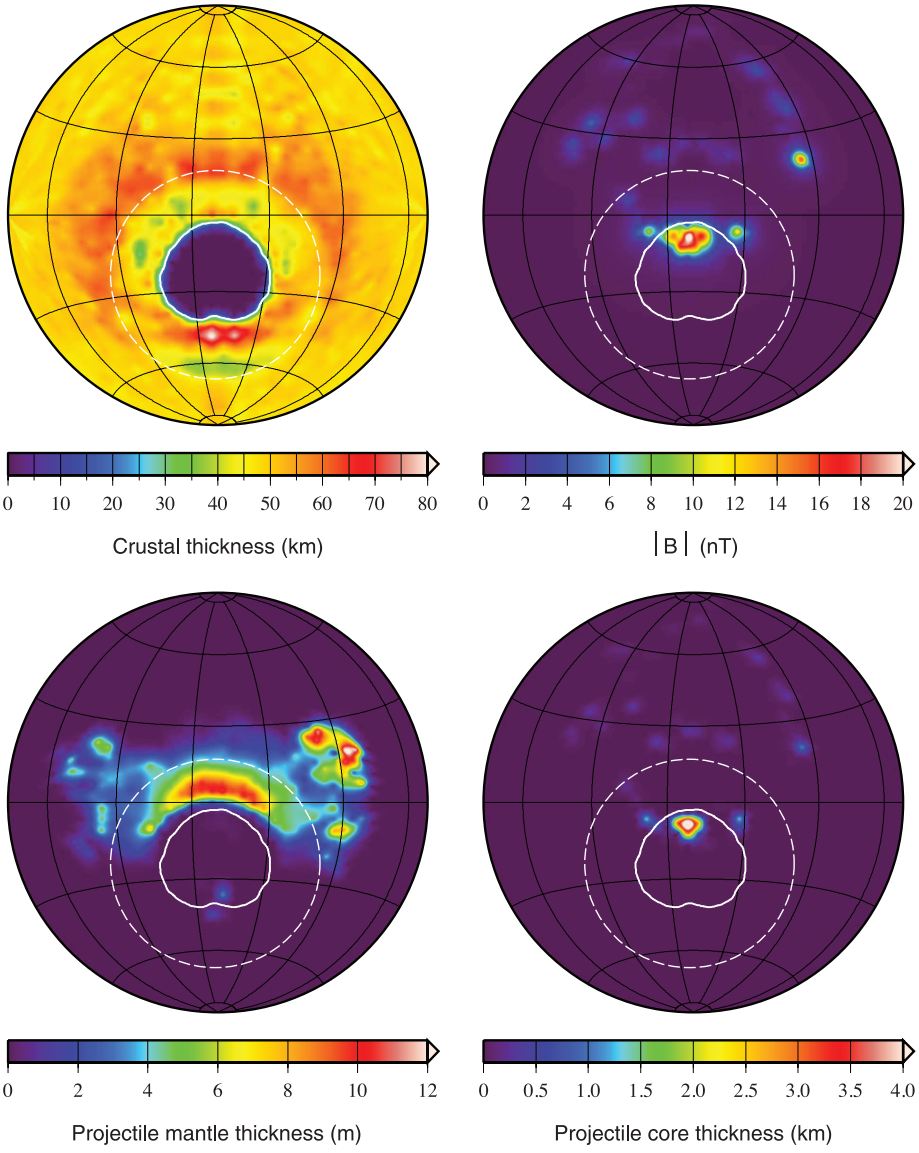

Fig. 3. Crustal thickness (top left), predicted magnetic field strength |*B*| (top right), integrated thickness of projectile mantle materials (bottom left), and integrated thickness of projectile core materials (bottom right) for a representative impact event sufficient to form the South Pole–Aitken basin. This oblique impact simulation used a differentiated projectile 200 km in diameter with a core 110 km in diameter. The impact direction was from south to north, the impact velocity was 15 km s^{-1}, and the impact angle from vertical was 45°. The projectile component delivered to the Moon acquired a thermoremanent magnetization in a dipolar field with a surface field strength of 5 μT. All images show half of the lunar surface and are displayed in a Lambert azimuthal equal-area projection. The solid white contour denotes where the crustal thickness has been reduced by a factor of 2 and is an approximate boundary for the extent of the deep melt sheet; the dashed outer ellipse is an approximation of the location of the final basin rim.

and 260 km (figs. S1 to S4). The overall distribution and thickness of proximal ejecta materials differed by a factor of ~3, depending on resolution, which is small in comparison to the uncertainty in the magnetic paleofield strength. For impact angles of 30° from vertical, the projectile core materials were deposited in the central portion of the basin, where they can sink through the melt sheet. For impact angles of 60° from vertical, a larger fraction of the projectile escaped the Moon's gravity, and the projectile core materials were deposited exterior to the basin rim. For homogeneous projectiles (figs. S5 to S8), the projectile materials were deposited farther downrange than for a similar impact of a differentiated projectile. If the projectile materials had the magnetic properties of average chondritic meteorites, dipole field strengths of 100 μT would generate magnetic anomalies that are similar to those observed on the Moon. Larger impact velocities favor projectile vaporization, leading to weaker magnetic anomalies. Although both differentiated and undifferentiated projectiles can account for the distribution and intensities of lunar magnetic anomalies, differentiated projectiles with impact angles of 45° most easily account for the strong anomalies that are located near the rim of the South Pole–Aitken basin. In our simulations, some projectile materials were deposited far from the basin rim, and this distal ejecta could potentially explain the existence of strong isolated anomalies on the lunar nearside, such as Reiner-γ and Descartes (Fig. 1).

Large impact events were common in the early evolution of the solar system, and these would certainly have accreted important quantities of highly magnetic materials to the crusts of all the terrestrial planets and moons. A giant northern lowlands–forming oblique impact on Mars (*30*, *31*) could help to explain the existence of strong crustal magnetic anomalies in the southern highlands of Mars that are otherwise difficult to understand (*32*, *33*). Similar magnetic anomalies might be expected to surround the Caloris basin on Mercury. Impact basin–associated magnetic anomalies should scale with the amount of retained projectile materials, and hence with basin size. Being exogenic in origin, planetary magnetic anomalies could be used to search for ancient meteoritic materials.

References and Notes

1. P. Dyal, C. W. Parkin, W. D. Daily, *Rev. Geophys. Space Phys.* **12**, 568 (1974).
2. L. Hood *et al.*, *J. Geophys. Res.* **106**, 27825 (2001).
3. D. L. Mitchell *et al.*, *Icarus* **194**, 401 (2008).
4. M. E. Purucker, J. B. Nicholas, *J. Geophys. Res.* **115**, E12007 (2010).
5. M. Fuller, S. M. Cisowski, in *Geomagnetism*, J. A. Jacobs, Ed. (Academic Press, London, 1987), vol. 2, pp. 307–455.
6. J. Gattacceca *et al.*, *Earth Planet. Sci. Lett.* **299**, 42 (2010).
7. W. D. Daily, P. Dyal, *Phys. Earth Planet. Inter.* **20**, 255 (1979).
8. L. L. Hood, Z. Huang, *J. Geophys. Res.* **96**, 9837 (1991).
9. D. Crawford, P. Schultz, *Int. J. Impact Eng.* **23**, 169 (1999).
10. D. R. Stegman, A. M. Jellinek, S. A. Zatman, J. R. Baumgardner, M. A. Richards, *Nature* **421**, 143 (2003).
11. M. A. Wieczorek *et al.*, *Rev. Mineral. Geochem.* **60**, 221 (2006).
12. M. Le Bars, M. A. Wieczorek, Ö. Karatekin, D. Cébron, M. Laneuville, *Nature* **479**, 215 (2011).
13. C. A. Dwyer, D. J. Stevenson, F. Nimmo, *Nature* **479**, 212 (2011).
14. L. Hood, *Icarus* **211**, 1109 (2011).
15. J. Halekas, R. Lin, D. Mitchell, *Meteorit. Planet. Sci.* **38**, 565 (2003).
16. J. Halekas *et al.*, *J. Geophys. Res.* **106**, 27841 (2001).
17. L. Hood, N. Artemieva, *Icarus* **193**, 485 (2008).
18. D. Wang, R. Van der Voo, D. R. Peacor, *Geosphere* **1**, 138 (2005).
19. P. Rochette, J. Gattacceca, A. V. Ivanov, M. A. Nazarov, N. S. Bezaeva, *Earth Planet. Sci. Lett.* **292**, 383 (2010).
20. I. Garrick-Bethell, B. P. Weiss, D. L. Shuster, J. Buz, *Science* **323**, 356 (2009).
21. E. K. Shea *et al.*, *Science* **335**, 453 (2012).
22. R. L. Korotev, *J. Geophys. Res.* **105**, 4317 (2000).
23. I. Garrick-Bethell, M. T. Zuber, *Icarus* **204**, 399 (2009).
24. R. Tagle, L. Hecht, *Meteorit. Planet. Sci.* **41**, 1721 (2006).
25. R. Tagle, R. T. Schmitt, J. Erzinger, *Geochim. Cosmochim. Acta* **73**, 4891 (2009).
26. R. L. Korotev, *J. Geophys. Res.* **92**, E491 (1987).
27. E. Pierazzo, H. J. Melosh, *Meteorit. Planet. Sci.* **35**, 117 (2000).
28. L. E. Senft, S. Stewart, *Earth Planet. Sci. Lett.* **287**, 471 (2009).
29. A. Brecher, L. Albright, *J. Geomag. Geoelectr.* **29**, 379 (1977).
30. J. C. Andrews-Hanna, M. T. Zuber, W. B. Banerdt, *Nature* **453**, 1212 (2008).
31. M. M. Marinova, O. Aharonson, E. Asphaug, *Nature* **453**, 1216 (2008).
32. J. E. P. Connerney *et al.*, *Geophys. Res. Lett.* **28**, 4015 (2001).
33. D. J. Dunlop, J. Arkani-Hamed, *J. Geophys. Res.* **110**, E12S04 (2005).
34. D. E. Smith *et al.*, *Geophys. Res. Lett.* **37**, L18204 (2010).

Acknowledgments: Supported by CNRS, the MIT-France Seed Funds program, the NASA Lunar Science Institute, and the NASA Lunar Advanced Science and Exploration Research Program. The cratering calculations were run on the Odyssey cluster supported by the FAS Science Division Research Computing Group at Harvard University. We thank B. Carbone for administrative help. All author modifications of the CTH code (available by licensing from Sandia National Laboratory) are available upon request.

Supporting Online Material

www.sciencemag.org/cgi/content/full/335/6073/1212/DC1
SOM Text
Figs. S1 to S8
Tables S1 to S4
References (*35*–*86*)

3 October 2011; accepted 30 January 2012
10.1126/science.1214773

Reconstruction of *Microraptor* and the Evolution of Iridescent Plumage

Quanguo Li,[1] Ke-Qin Gao,[2] Qingjin Meng,[1] Julia A. Clarke,[3] Matthew D. Shawkey,[4]* Liliana D'Alba,[4] Rui Pei,[5] Mick Ellison,[5] Mark A. Norell,[5] Jakob Vinther[3,6]

Iridescent feather colors involved in displays of many extant birds are produced by nanoscale arrays of melanin-containing organelles (melanosomes). Data relevant to the evolution of these colors and the properties of melanosomes involved in their generation have been limited. A data set sampling variables of extant avian melanosomes reveals that those forming most iridescent arrays are distinctly narrow. Quantitative comparison of these data with melanosome imprints densely sampled from a previously unknown specimen of the Early Cretaceous feathered *Microraptor* predicts that its plumage was predominantly iridescent. The capacity for simple iridescent arrays is thus minimally inferred in paravian dinosaurs. This finding and estimation of *Microraptor* feathering consistent with an ornamental function for the tail suggest a centrality for signaling in early evolution of plumage and feather color.

Feather colors in extant birds (Aves) are generated from pigments and a variety of nanostructural architectures (*1*, *2*). Iridescent colors, an integral part of the avian plumage color gamut involved in signaling and display, are produced through coherent light scattering by laminar or crystal-like arrays generated by layers of materials with different refractive indices—namely, keratin, melanin, and sometimes air—in feather barbules (*1*, *2*). Melanosomes can be arranged in single or multiple layers (*1*, *2*), and recent work shows that even slight organization of melanosomes can produce weakly iridescent (glossy) colors (*3*). Iridescent nanostructures are diverse and have evolved independently numerous times in extant birds (*4*), but whether they are exclusively avian innovations or appear earlier in dinosaur evolution has been unknown.

Thus far, fossil evidence of iridescent plumage has been limited to a 47-million-year-old isolated avian feather from Germany (Grube Messel) (*5*). This feather preserved in fine nanostructural detail the organization typical of many iridescent avian melanosome arrays. Such pristine preservation is rare, however, and so far unknown in

[1]Beijing Museum of Natural History, 126 Tianqiao South Street, Beijing 100050, People's Republic of China. [2]School of Earth and Space Sciences, Peking University, Beijing 100871, People's Republic of China. [3]Department of Geological Sciences, University of Texas at Austin, 1 University Station C1100, Austin, TX 78712, USA. [4]Department of Biology and Integrated Bioscience Program, University of Akron, Akron, OH 44325–3908, USA. [5]Department of Paleontology, American Museum of Natural History, 79th Street at Central Park West, New York, NY 10024, USA. [6]Department of Geology and Geophysics, Yale University, New Haven, CT 06520–8109, USA.

*To whom correspondence should be addressed. E-mail: shawkey@uakron.edu